THE JOURNAL OF BIOLOGICAL CHEMISTRY VOL. 285, NO. 17, pp. 13045–13056, April 23, 2010

Kidney-specific Overexpression of Sirt1 Protects against Acute Kidney Injury by Retaining Peroxisome Function[S]

Received for publication, September 19, 2009, and in revised form, January 11, 2010 Published, JBC Papers in Press, February 5, 2010, DOI 10.1074/jbc.M109.067728

Kazuhiro Hasegawa[‡], Shu Wakino[‡1], Kyoko Yoshioka[‡], Satoru Tatematsu[‡], Yoshikazu Hara[‡], Hitoshi Minakuchi[‡], Keiko Sueyasu[‡], Naoki Washida[‡], Hirobumi Tokuyama[‡], Maty Tzukerman[§], Karl Skorecki[§], Koichi Hayashi[‡], and Hiroshi Itoh[‡]

From the [‡]Department of Internal Medicine, School of Medicine, Keio University, Tokyo 160-8582, Japan and the [§]Rappaport Faculty of Medicine and Research Institute, Technion-Israel Institute of Technology, Haifa 31096, Israel

Sirt1, a NAD-dependent protein deacetylase, is reported to regulate intracellular metabolism and attenuate reactive oxidative species (ROS)-induced apoptosis leading to longevity and acute stress resistance. We created transgenic (TG) mice with kidney-specific overexpression of Sirt1 using the promoter sodium-phosphate cotransporter IIa (Npt2) driven specifically in proximal tubules and investigated the kidney-specific role of Sirt1 in the protection against acute kidney injury (AKI). We also elucidated the role of number or function of peroxisome and mitochondria in mediating the mechanisms for renal protective effects of Sirt1 in AKI. Cisplatin-induced AKI decreased the number and function of peroxisomes as well as mitochondria and led to increased local levels of ROS production and renal tubular apoptotic cells. TG mice treated with cisplatin mitigated AKI, local ROS, and renal tubular apoptotic tubular cells. Consistent with these results, TG mice treated with cisplatin also exhibited recovery of peroxisome number and function, as well as rescued mitochondrial function; however, mitochondrial number was not recovered. Immunoelectron microscopic findings consistently demonstrated that the decrease in peroxisome number by cisplatin in wild type mice was restored in transgenic mice. In HK-2 cells, a cultured proximal tubule cell line, overexpression of Sirt1 rescued the cisplatin-induced cell apoptosis through the restoration of peroxisome number, although the mitochondria number was not restored. These results indicate that Sirt1 overexpression in proximal tubules rescues cisplatin-induced AKI by maintaining peroxisomes number and function, concomitant up-regulation of catalase, and elimination of renal ROS levels. Renal Sirt1 can be a potential therapeutic target for the treatment of AKI.

Sir2 (silent information regulator 2), a family of NAD-dependent protein deacetylases, can deacetylate various substrates involved in metabolism, acute stress resistance, and longevity (1). Sirt1, a mammalian homologue of Sir2, acts on several nuclear proteins, including p53 (2) and forkhead family proteins (FoxOs) (3), and prevents apoptosis. Calorie restriction or resveratrol, which activates Sirt1, is reported to protect from reactive oxygen species (ROS)-induced[2] organ insult (4, 5). Additionally, the overexpression of Sirt1 itself also strengthens the stress resistance. For example, in mice with heart-specific Sirt1 overexpression, ROS-induced cardiac apoptosis was attenuated (6). Furthermore, we have recently demonstrated that Sirt1 in cultured proximal tubular cells alleviates H_2O_2-induced apoptosis (7). However, the direct relationship between kidney-specific Sirt1 and renal tissue survival *in vivo* has not been elucidated.

Several mechanisms have been suggested for the role of Sirt1 in apoptosis and/or oxidative stress. We have elucidated that Sirt1 activates catalase, which helps protect against ROS-induced injury (7). Transgenic (TG) mice overexpressing catalase in proximal renal tubular cells manifest attenuated renal tubular apoptosis (8). Liver-specific Sirt1 knock-out mice showed that Sirt1 activates fatty acid oxidation (FAO) (9). Because both peroxisomes and mitochondria play a significant role in FAO, and catalase is mainly localized in peroxisomes, it is surmised that Sirt1 also influences not only mitochondria but also peroxisomes. However, the direct relationship between Sirt1 and peroxisomes has not been examined thus far. Furthermore, Sirt1 has been reported to preserve mitochondria function by inducing PGC-1α, which increases mitochondrial number (10). Because both peroxisome and mitochondrial functions are compromised by pathophysiological conditions, including cisplatin-induced (11, 12) and ischemic/reperfusion (I/R)-induced acute kidney injury (AKI) (13, 14), it is anticipated that Sirt1 is capable of alleviating renal injury by modulating peroxisome and mitochondrial function.

To examine the role of Sirt1 in renal tubules, we produced TG mice overexpressing Sirt1 specifically in proximal tubules. These mice were subjected to cisplatin- or I/R-induced AKI to investigate whether Sirt1 rescued renal insults. We also attempted to elucidate the role of peroxisome as well as mitochondria in mediating the mechanisms for the renal protective effects of Sirt1 in AKI.

[S] The on-line version of this article (available at http://www.jbc.org) contains supplemental Tables SI–SIII and Figs. SI–SV.

[1] To whom correspondence should be addressed: Dept. of Internal Medicine, School of Medicine, Keio University, 35 Shinanomachi, Shinjuku-ku, Tokyo 160-8582, Japan. Tel.: 81-3-5363-3796; Fax: 81-3-3359-2745; E-mail: swakino@sc.itc.keio.ac.jp.

[2] The abbreviations used are: ROS, reactive oxidative species; TG, transgenic; AKI, acute kidney injury; WT, wild type; FAO, fatty acid oxidation; I/R, ischemic/reperfusion; BUN, blood urea nitrogen; mtDNA, mitochondrial DNA; PMP70, 70-kDa peroxisomal membrane protein; ACOX1, peroxisome acyl-CoA oxidase; MCAD, medium chain acyl-CoA dehydrogenase; PPAR, peroxisome proliferator-activated receptor; PGC-1α, PPARγ cofactor-1α; 4-HNE, 4-hydroxy-2(E)-nonenal; TUNEL, terminal deoxynucleotidyltransferase-mediated dUTP nick end labeling; immuno-EM, immunoelectron microscopy; CR, calorie restriction; NC, normal chow; FACS, fluorescence-activated cell sorter; AQP4, aquaporin 4.

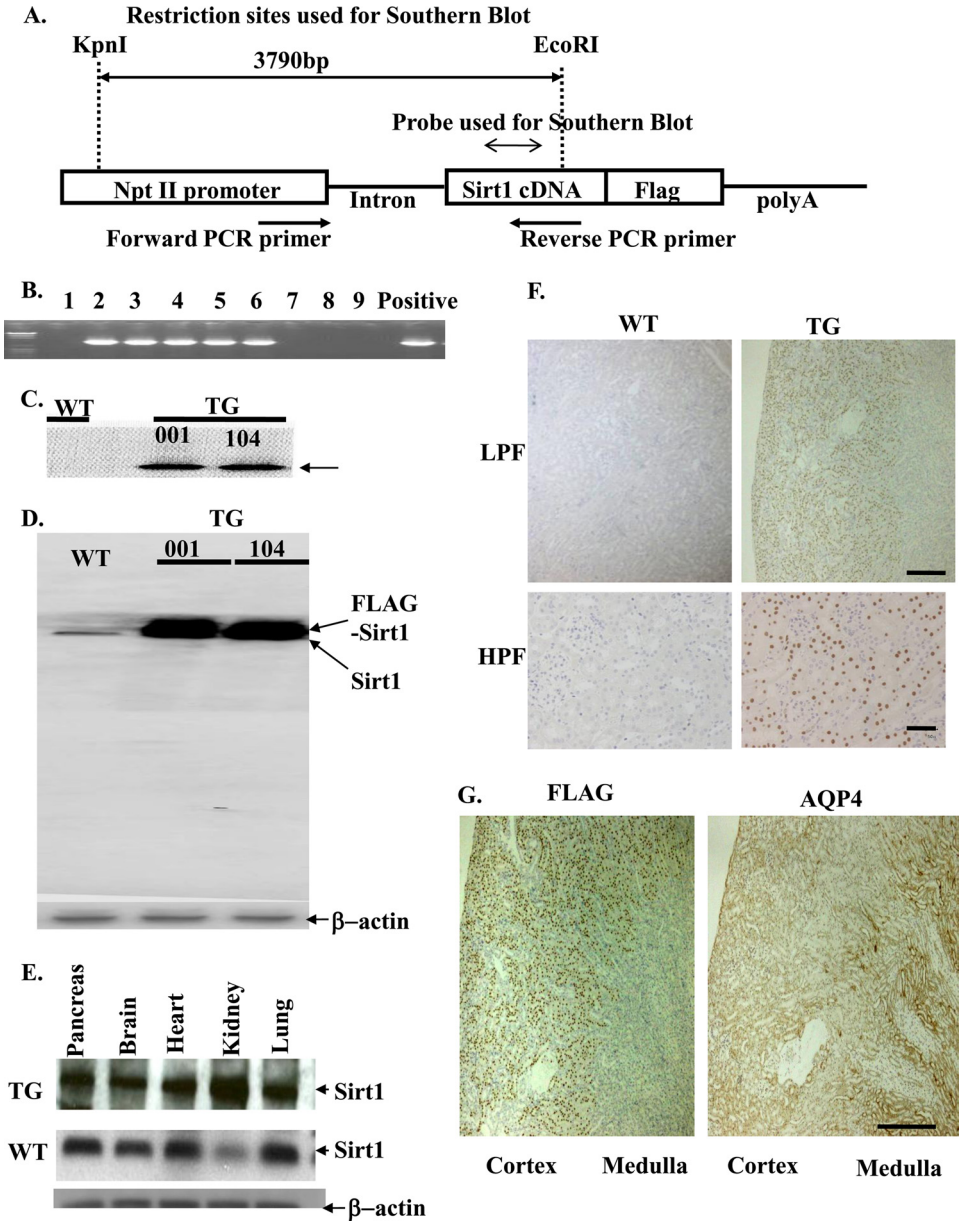

FIGURE 1. **Foundation of renal tubule-specific Sirt1 TG mice.** *A*, the construct used for the foundation of kidney-specific Sirt1 TG mice contains a fragment from the Npt II promoter, a human Sirt1 cDNA fragment, a FLAG tag sequence, an intron, and β-globin polyadenylation sequences. The restriction sites or probes used in the Southern blot and PCR primers are indicated. Sequences of primers designed for the of Southern blot probe are listed in supplemental Table SI. *B*, a PCR analysis for genotyping of TG mice. We used the transgenic vector including human kidney cDNA as a positive control. *C*, Southern blotting shows the introduction of Sirt1 transgene in mice of line 001 and 104. An *arrow* indicates a band corresponding to transgene-derived Sirt1. *D*, immunoblotting for Sirt1 indicates that TG mice express approximately five times the level of Sirt1 as compared with WT mice. *E*, Sirt1 expressions in various tissues from TG mice. *F*, immunohistochemical localization of Sirt1 shows predominant expression in proximal tubules in kidneys of TG mice. Kidneys from TG and WT mice were immunostained for FLAG epitope as described under "Experimental Procedures." Original magnification was ×100 (*LPF*) or ×400 (*HPF*). *Scale bars* indicate 500 μm (low power field; *LPF*) and 100 μm (high power field; *HPF*). *G*, kidneys from mice overexpressing Sirt1 demonstrate that Sirt1 is overexpressed preferentially in the cortical area (proximal S1 + S2 segments). The immunohistological examination reveals no overlap between Sirt1 and AQP-4 staining areas (proximal S3 segments). They are from sequential sections labeled with anti-Sirt1 and anti-AQP4 antibody. *Scale bar*, 500 μm.

EXPERIMENTAL PROCEDURES

Experimental Protocol for AKI—Eight-week-old male mice were used in these experiments. For the induction of cisplatin-induced AKI, the mice were given intraperitoneal saline or cisplatin infusion (20 mg/kg/day; Sigma) for 3 days. On the third day, the kidney was harvested for histological analysis, and blood was taken for laboratory assay.

For the induction of I/R renal injury, the kidney was subjected to ischemia by clamping both renal pedicles for 60 min with vascular clips (Roboz, Gaithersburg, MD), during which the mice were kept at constant temperature (37 °C) with a warm blanket and well hydrated. Then the clip was removed, which allowed for reperfusion. After 24 h of renal ischemia, the kidney tissues were removed, and serum samples were obtained. A sham operation was performed by manipulation of the renal pedicles without clamping. Four animals from each respective genotype were used for each experiment. Serum levels of blood urea nitrogen (BUN) and creatinine were measured with Fujifilm DRI-CHEM3500V autoanalyzer (Fuji Photo Film). These studies as well as the following animal studies were performed in accordance with the animal experimentation guidelines of Keio University School of Medicine.

Experimental Protocol for Calorie Restriction—Calorie restriction was performed as described previously (15). Ten male C57BL/6 mice were randomly assigned to two groups of five. From two months of age, one group was fed normal chow, and the other group was put on a caloric restriction diet (70% of calorie intake adjusted to body weight) for three months. At the end of five months, the effects of cisplatin on the kidneys from calorie-restricted mice were evaluated. The mice were sacrificed, and the kidneys were removed for use in immunoblotting and histological experiments as described below.

Plasmids and Constructs—Human Sirt1 cDNA containing its full-length open reading frame was cloned as described previously (16). In constructing the transgenic expression vector, the cDNA for Sirt1 was followed by an eight-amino acid FLAG epitope (Invitrogen). To generate renal tubular epithelium-specific TG mouse, the sequence for human Sirt1 cDNA with FLAG epitope was ligated with mouse sodium phosphate cotransporter IIa (Npt2) promoter (17), and this clone was designated as Npt2-Sirt1-FLAG (see Fig. 1*A*).

Generation of Renal Tubular-specific Sirt1 TG Mice—To generate TG mice, the SalI-NotI fragment of Npt2-Sirt1-FLAG was microinjected into one-cell fertilized mouse embryos

obtained from superovulated C57BL/6 × C3H mice (see Fig. 1*A*) (18). Founder mice were identified by Southern blot analysis of KpnI/EcoRI-digested tail genomic DNA with the human Sirt1 cDNA as a probe. The PCR primers for making Southern blot probes are listed in supplemental Table SI. The positive TG founders were then crossed with wild type C57BL/6 mice (Charles River Japan Inc.) to obtain the F1 generation. Genomic DNA was isolated from tail biopsies at 3 weeks of age using a DNeasy kit (Qiagen) and subjected to Southern blot analysis to identify the transgene. Southern blots were performed using a ^{32}P-labeled probe of human Sirt1 cDNA. Genomic DNA digested by KpnI and EcoRI yielded a single band of the expected size in TG mice only (see Fig. 1*C*). Additional screening of genomic DNA samples was performed by polymerase chain reaction using the transgene-specific oligonucleotide primers CTATGCTGAGGCCCTAGGTTC TAT (Npt2 promoter side) and GTCGTCGTCTTCGTCGTACAAGTTG (Sirt1 gene side) (see Fig. 1*A*), which amplify a 1310-bp region spanning the junction between the Npt2 promoter and the Sirt1 gene (see Fig. 1*B*). We used the transgenic vector as a positive control.

Quantification of Mitochondrial DNA (mtDNA)—Total RNA from mouse kidneys were prepared as described previously (19). The LightCycler Instrument (Roche Applied Science) was used for the quantification of mtDNA with hybridization probes in a total volume of 20 μl, containing 0.5 μM of each primer, 0.2 μM of each probe, 5 mM $MgCl_2$, 2 μl of Light Cycler-DNA Master hybridization probes (Roche Applied Science), and 20 ng of DNA. The cycling conditions were set as follows: initial denaturation 95 °C for 30 s (temperature transition rate, 20 °C/s) followed by 45 cycles of 95 °C for 0 s (20 °C/s), 53 °C for 5 s (20 °C/s), and 72 °C for 11 s (2 °C/s). The standard curve was calculated by analyzing serial dilutions (0.64–5.0 × 10^4 pg/μl) of plasmid DNA inserted with the target PCR product. The mtDNA contents of kidney tissues were normalized to the total amount of DNA in each sample. The primers and probes were as follows: sense primer, 5′-ACCATTTGCAGACGCCATAA-3′; antisense primer, 5′-TGAAATTGTTTGGGCTACGG-3′; 3′-fluorescein-labeled anchor probe, 5′-CATCTAGCCTATCAGTTTACTCCATTCT-3′; and 5′-LC Red 640-labeled sensor probe, 5′-TGATCAGGATGAGCCTCAAACTCCAAAT-3′. These primers and probes were designed to amplify the mouse mtDNA designed in reference to the *Mus musculus* mitochondrion genome and not to amplify the mtDNA-like sequence in the nuclear genome.

Immunoblotting—Immunoblotting was performed as described previously (19) using specific antibodies against Sirt1 (Millipore, Bedford, MA), catalase (Calbiochem, La Jolla, CA), 70-kDa peroxisomal membrane protein (PMP70; Affinity Bioreagents, Golden, CO), peroxisome acyl-CoA oxidase (ACOX1; Abcam Inc., Cambridge, MA), medium chain acyl-CoA dehydrogenase (MCAD; Cayman Chemicals, Ann Arbor, MI), and PPARγ cofactor-1α (PGC-1α; Santa Cruz Biotechnology, Santa Cruz, CA). The anti-Sirt1 antibody was generated from rabbit and recognizes both human and mouse Sirt1. The β-actin band recognized by specific antibody (Sigma) was used as a loading control. For immunoblotting, 30 μg of protein from each sample was loaded into the individual lanes of the gels.

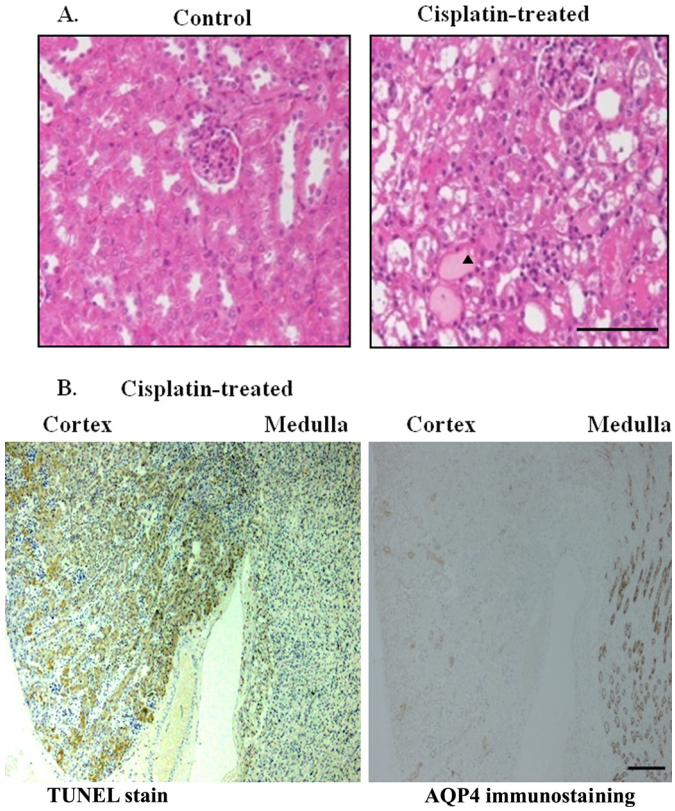

FIGURE 2. **Effects of cisplatin on renal histology and apoptotic process.** *A*, renal histological changes induced by cisplatin-induced acute kidney injury. AN *arrowhead* indicates the areas of cisplatin-induced damages. *Scale bar*, 100 μm. *B*, TUNEL-positive cells are detected in cortical areas, which barely overlap with areas containing cells expressing AQP4 (a marker for proximal S3 segments) in mice treated with cisplatin. They are from sequential sections labeled with anti-AQP4 antibody and stained with TUNEL. *Scale bar*, 200 μm.

Immunohistochemistry—Four-μm paraffin sections of kidneys were used to stain for aquaporin 4 (AQP4), 4-hydroxy-2(E)-nonenal (4-HNE), Sirt1, and FLAG, using primary antibodies including anti-AQP4 antibody (Santa Cruz Biotechnology), 4-HNE (Japan Institute for the Control of Aging), Sirt1 (Millipore, Bedford, MA), and FLAG (Sigma). Tissue sections of 4-μm thickness were obtained and fixed in 3% formaldehyde in phosphate-buffered saline for 15 min at room temperature and treated as described previously (20). Briefly, the sections were sequentially blocked for endogenous biotin binding using a Vector blocking kit (Vector Laboratories, Burlingame, CA) and for endogenous peroxidase activity with 1.5% H_2O_2, 0.2 mol/liter Na_3N in Hanks' balanced salt solution with 0.01 mol/liter HEPES (HBSS-HEPES) with 0.1% saponin. Nonspecific binding was blocked with 10% normal goat serum. After incubation with preimmune or immune sera overnight, the sections were stained with biotin-labeled goat anti-rabbit IgG (Vector) or biotin-labeled anti-mouse IgG (Vector) and then treated with the Vecstatin Elite ABC Kit (Vector). The slides were washed with HBSS-HEPES and developed with 3,3′-diaminobenzidine tetrahydrochloride substrate (0.5 mg/ml) in 0.05 mol/l Tris, pH 7.4, 0.0075% H_2O_2 (Sigma).

RNA Isolation, Reverse Transcription, and Quantitative PCR—Total RNA was isolated using TRIzol reagent (Invitrogen). RNA (400 ng) was reverse transcribed to cDNA using the SuperScript II

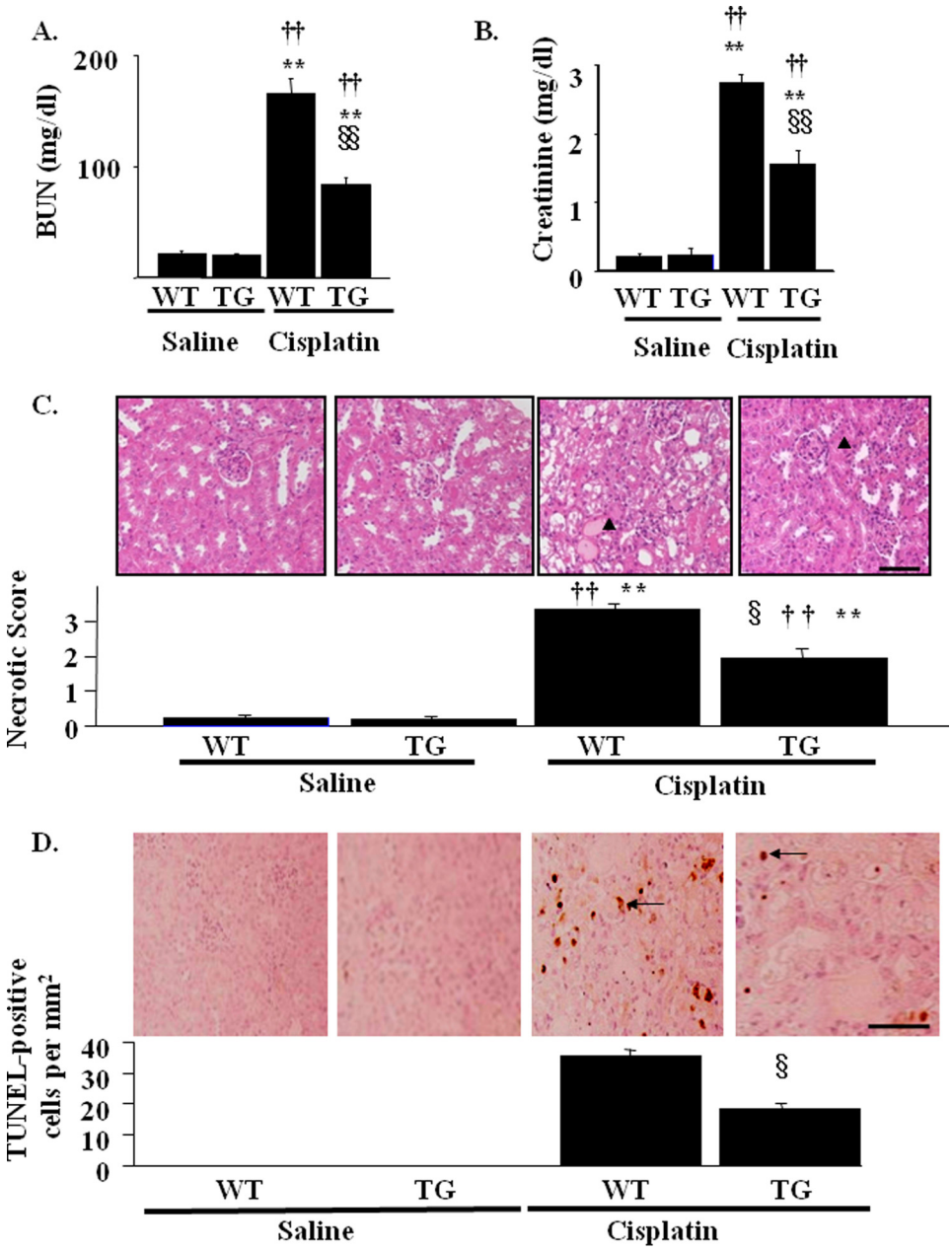

FIGURE 3. **Effects of kidney-specific Sirt1 overexpression on renal function and histology in cisplatin-induced acute kidney injury.** *A* and *B*, WT or TG mice was treated with cisplatin as described under "Experimental Procedures." Serum levels of BUN (*A*) and creatinine (*B*) were measured 3 days after cisplatin injection. *C*, representative hematoxylin-eosin staining of kidney sections from WT and TG mice in cisplatin-induced AKI. An *arrowhead* represents lysed tubules. Pathological scores of tubular damages as described under "Experimental Procedures" are shown in the *lower panel*. *Scale bar*, 100 μm. *D*, representative images of the TUNEL assay show cisplatin-induced renal tubular cell apoptosis in WT mice, which is attenuated in TG mice. An *arrow* indicates TUNEL-positive cells with condensed or fragmented nuclei. The numbers of TUNEL-positive cells are shown in the *lower panel*. *Scale bar*, 100 μm. *, $p < 0.05$ *versus* saline-infused WT mice; **, $p < 0.01$ *versus* saline-infused WT mice; †, $p < 0.05$ *versus* saline-infused TG mice; ††, $p < 0.01$ *versus* saline-infused TG mice; §, $p < 0.05$ *versus* cisplatin-infused WT mice; §§, $p < 0.01$ *versus* cisplatin-infused WT mice ($n = 4$).

RNase H-Reverse Transcriptase system (Invitrogen), and specific transcripts were quantitated by real time PCR using the ABI Prism 7700 sequence detection system (Applied Biosystems, Foster City, CA) and the SYBR GREEN system (Applied Biosystems). Sequences of the primers are listed in supplemental Tables SII and SIII. The relative mRNA levels for the specific genes were normalized to 28 S rRNA levels. The reference gene (28 S rRNA) was not affected by cisplatin treatment.

Renal Histology—After the kidneys were removed, they were fixed in 4% parformaldehyde for paraffin embedding. Paraffin-embedded tissues were sectioned at 4 μm for hematoxylin and eosin staining. Renal histology was examined in a blinded fashion. The following histological changes were evaluated: the percentage of renal tubules that displayed cell lysis, the loss of brush border, and cast formation. The development of tissue damage was scored as follows; 0, no damage; 1, <25% damage; 2, 25–50% damage; 3, 50–75% damage; 4, >75% damage. Pictures of representative fields were also recorded.

TUNEL Assay—Apoptosis of renal tubular cells was identified by TUNEL assay as described previously (18) with an *in situ* cell death detection kit (Roche Applied Science).

Quantification of Peroxisomes and Mitochondria by Immunoelectron Microscopy—For postembedding immunoelectron microscopy (immuno-EM), sliced kidney sections were fixed for 1 h at room temperature with 4% formaldehyde and 0.25% glutaraldehyde in 0.1 M HEPES/NaOH, pH 7.4. After rapid dehydration in ethanol, the sections were embedded in LR White embedding resin. Thin sections on nickel grids were preincubated on a drop of 0.5% bovine serum albumin in phosphate-buffered saline. The sections were incubated overnight in the 1/1000 diluted primary antibody, an anti-PMP70 antibody. After being rinsed with phosphate-buffered saline, the sections were incubated for 30 min on a drop of protein A-gold (15 nm) prepared as described previously (21). The sections were briefly contrasted with uranyl acetate and lead citrate before examination. Eight random ultrastructural photomicrographs taken on the microscopic fields corresponding to the kidney cortex area from each mice at a magnification of ×12,800 were chosen for observation. Then peroxisomes and mitochondria were numbered. By the above postembedding protein A gold labeling, anti-PMP70 antibody gave specific signals on the membranes of peroxisomes, whereas mitochondria were negative on staining with the anti-PMP 70 antibody.

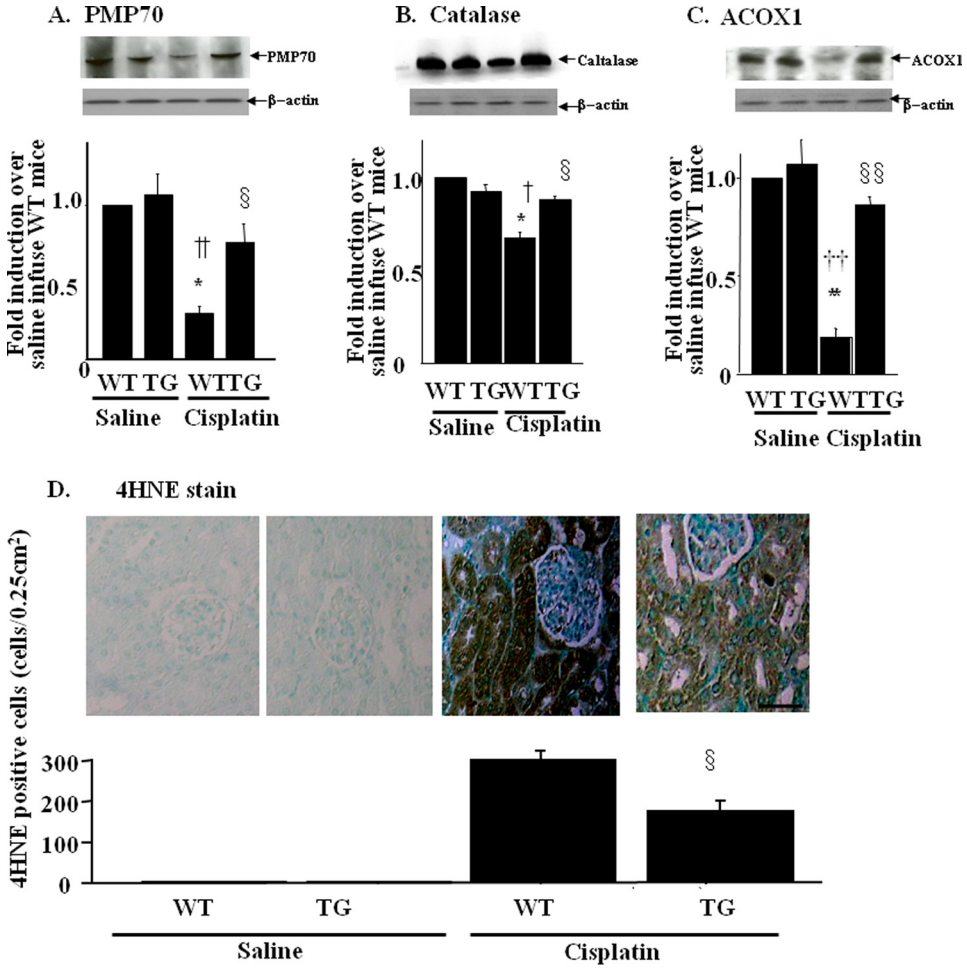

FIGURE 4. **Effects of kidney-specific Sirt1 overexpression on peroxisome number and function and on local ROS production in cisplatin-induced acute kidney injury.** *A–C*, the expression levels of peroxisome protein, PMP-70 (*A*), catalase (*B*), and ACOX1 (*C*) are analyzed by immunoblotting using kidney lysates from WT and TG mice 3 days after saline or cisplatin injection. The *bar graphs* in the *lower panels* show the quantification of the band intensity. *D*, local ROS production is assayed by 4-HNE immunostaining. The staining is mainly observed in the proximal tubules in the kidney from WT mice with cisplatin treatment, but is attenuated in those from TG mice. *Scale bar*, 50 μm. *, $p < 0.05$ *versus* saline-infused WT mice; **, $p < 0.01$ *versus* saline-infused WT mice; †, $p < 0.05$ *versus* saline-infused TG mice; ††, $p < 0.01$ *versus* saline-infused TG mice; §, $p < 0.05$ *versus* cisplatin-infused WT mice; §§, $p < 0.01$ *versus* cisplatin-infused WT mice ($n = 4$).

Tissue Culture—HK2 cells were cultured as previously described (7). The expression plasmid containing Sirt1 cDNA (pcDNA3.1-Sirt1) and the control plasmid (pcDNA3.1) were transfected into HK-2 cells by using Lipofectamine 2000 (Invitrogen) as described previously (7). Forty-eight hours after the transfection, the cells were used for the following experiments. Sirt1-transfected HK-2 cells were treated with or without cisplatin or I/R. Cisplatin was used at a dilution of 50 μM for 24 h in Dulbecco's modified Eagle's medium. In *in vitro* I/R experiments, HK-2 cells (~80% confluent) were washed in glucose-free buffer (154 mM NaCl, 5.6 mM KCl, 2.3 mM $CaCl_2$, 1.0 mM $MgCl_2$, 3.6 mM $NaHCO_3$, and 5 mM HEPES, pH 7.2) and then incubated with 10 mM antimycin A plus 10 mM 2-deoxyglucose plus 1 μM calcium ionophore (A23187) for 60 min (to induce ischemic injury *in vitro*). After this ischemic period, *in vitro* reperfusion was achieved by incubating cells in glucose-replete complete growth medium. Twelve hours later, the cells were harvested and subjected to the following study. The peroxisomal mass and the mitochondrial mass of HK2 cells were determined with the aid of the fluorescent dyes: Organelle Lights Peroxi-GFP and Organelle Lights Mito-OFP (Molecular Probes, Eugene, OR), respectively, following the manufacturer's instructions. For microscopic analysis, the HK2 cells were stained with the fluorescent probes and observed with a confocal microscope (LSM 510; Carl Zeiss, Oberkochen, Germany). In apoptosis measurements, annexin V-fluorescein isothiocyanate in combination with propiumiodine was used to quantitatively determine the percentage of cells undergoing apoptosis, as described previously (7).

Statistics—The data were expressed as the means ± S.E. The data were analyzed using one-way or two-way analysis of variance, as appropriate, followed by a Bonferroni's multiple comparison post hoc test. p values less than 0.05 were considered statistically significant.

RESULTS

Generation of Renal Epithelium-specific Sirt1 TG Mice—We generated TG mice with proximal tubule-specific overexpression of human Sirt1 by using Npt2 promoter (Fig. 1*A*). Positive TG mice were identified with PCR and confirmed by Southern blot (Fig. 1, *B* and *C*). We obtained two lines of TG mice, line 001 and line 104. The expression levels of Sirt1 in the kidney were similar between the two lines, and both lines developed normally and appeared to have the same phenotype. We used line 001 for subsequent experiments and showed the data below for the line 001. Immunoblotting showed that the Sirt1 band of TG mice was broad and composed of one band for endogenous Sirt1 (100 kDa) and one for FLAG-tagged human Sirt1 (101kD) (Fig. 1*D*). The protein expression levels of Sirt1 in TG mice were increased as compared with those in WT mice (Fig. 1*D*). TG mice were phenotypically normal and fertile. The overexpression of human Sirt1 in the kidney and other tissues was confirmed by immunoblotting (Fig. 1*E* and supplemental Fig. SI). Immunohistochemistry showed that exogenous transgene was overexpressed especially in the nucleus of renal tubular cells. (Fig. 1*F*). Sirt1 was localized preferentially in the cortical area, mostly likely in proximal S1 and S2 segments. In contrast, immunohistochemistry for Sirt1 revealed only modest staining in the medullary segments, and there was less overlap with the AQP4-expressing S3 segment area (Fig. 1*G*).

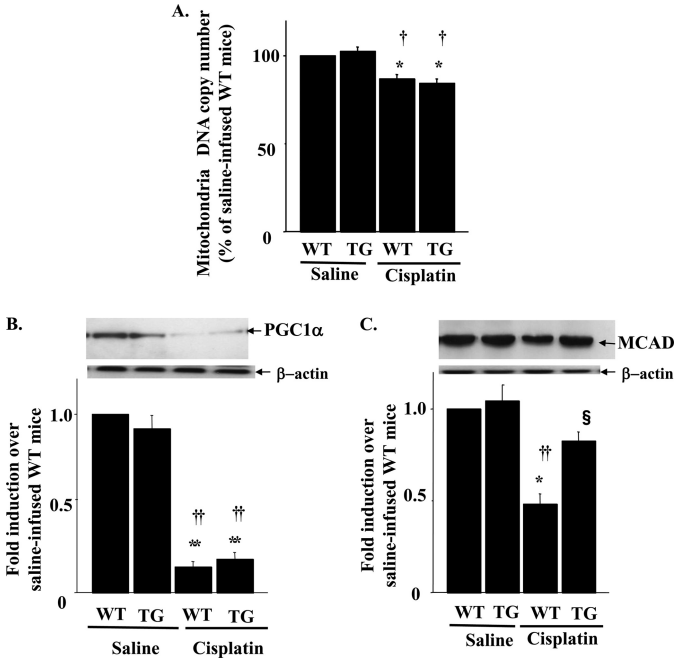

FIGURE 5. **Effects of kidney-specific Sirt1 overexpression on mitochondria number and function in cisplatin-induced acute kidney injury.** *A*, mitochondrial DNA copy number expressed as a percentage of control in kidney following cisplatin treatment. The expression levels of PGC-1α (*B*), a main activator of mitochondria biogenesis, and mitochodria protein MCAD (*C*) were examined by immunoblotting. The *upper panel* shows representative blotting, and the *lower panel* shows the results of the density analysis of each blot. *, $p < 0.05$ *versus* saline-infused WT mice; **, $p < 0.01$ *versus* saline-infused WT mice; †, $p < 0.05$ *versus* saline-infused TG mice; ††, $p < 0.01$ *versus* saline-infused TG mice; §, $p < 0.05$ *versus* cisplatin-infused WT mice ($n = 4$).

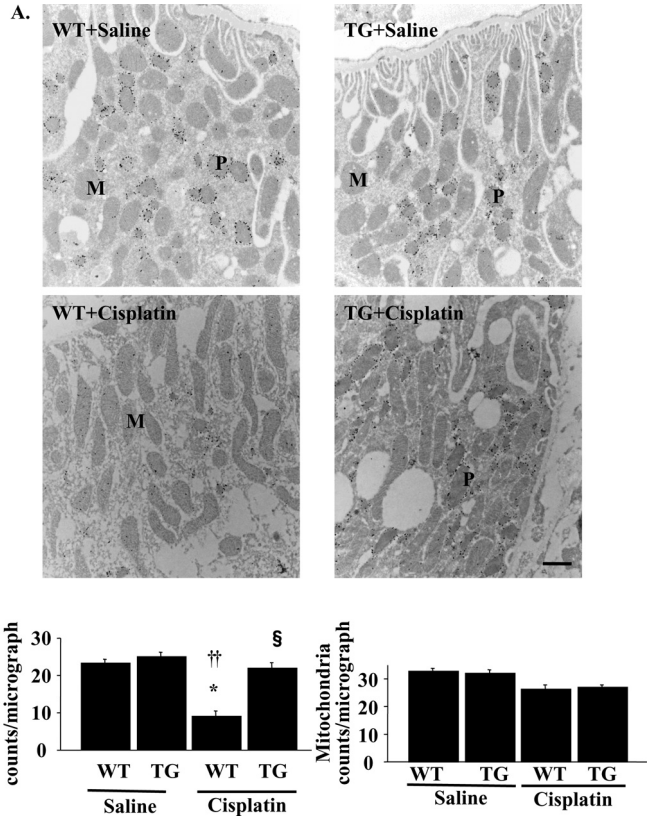

FIGURE 6. **Peroxisomal and mitochondrial numbers as evaluated in immuno-EM in cisplatin-induced acute kidney injury.** *A*, kidney tissue sections were prepared for ultrastructural analysis by immuno-EM using anti-PMP70 antibody. Representative kidney histopathology from WT and TG mice with saline or cisplatin are shown. WT and TG mice with saline showed similar numbers of peroxisomes (*P*) and mitochondria (*M*). WT mice with cisplatin showed decreased numbers of peroxisome, which were alleviated in TG mice with cisplatin. *Scale bar*, 1 μm. *B*, peroxisomal and mitochondrial number in the micrograph at the magnification of ×12,800 were calculated as described under "Experimental Procedures." *, $p < 0.05$ *versus* saline-infused WT mice; ††, $p < 0.01$ *versus* saline-infused TG mice; §, $p < 0.05$ *versus* cisplatin-infused WT mice ($n = 8$).

Cisplatin-induced AKI—After cisplatin injection, AKI developed with elevations in both BUN (166 ± 22 mg/dl, *versus* 21 ± 6 mg/dl, $p < 0.01$) and serum creatinine levels (2.7 ± 0.2 mg/dl *versus* 0.3 ± 0.1 mg/dl, $p < 0.01$) with renal tubular damage (Fig. 2*A*). Furthermore, TUNEL staining showed marked tubular cell apoptosis, particularly in cortical segments (Fig. 2*B*, *left panel*), which were adjacent to the AQP4-stained S3 segment of proximal tubules (Fig. 2*B*, *right panel*) (22). These data indicated that the areas affected by cisplatin in our experiment were predominantly localized in the S1+S2 segments.

Protective Effects of Sirt1 Overexpression on Cisplatin-induced AKI—The renal protective role of Sirt1 in cisplatin-induced AKI was examined in TG mice. The injection of cisplatin provoked AKI in WT mice, but AKI was partially ameliorated in TG mice (BUN, 83 ± 10 mg/dl; creatinine, 1.6 ± 0.4 mg/dl; Fig. 3, *A* and *B*, respectively). Concordantly, the renal histological changes induced by cisplatin were rescued in TG mice as evaluated by the pathological scores (Fig. 3*C*). To determine the effects of Sirt1 overexpression on renal cell apoptosis, we performed TUNEL staining. No TUNEL-positive cells were detected in both WT mice and TG mice with saline injection (Fig. 3*D*). In WT mice, cisplatin treatment resulted in an increase in TUNEL-positive cells (Fig. 3*D*, *arrows*), which was ameliorated in TG mice (TUNEL-positive cells, 35 ± 3/mm^2 *versus* 18 ± 3/mm^2 for WT and TG mice, respectively).

Effects of Sirt1 Overexpression on Peroxisome Function in Cisplatin-induced AKI—Cisplatin has been reported to decrease peroxisome number and impair its function (11), which contributes to the renal damage. To elucidate the role of Sirt1 in these changes, we examined the protein expression levels of PMP70, a marker for the number of peroxisome, as well as the levels of catalase and ACOX1, markers for peroxisomal function. As shown in Fig. 4*A*, cisplatin-treated mice exhibited ~70% reduction in PMP70 protein, which were restored in TG mice. Similar results were obtained with the expression levels of catalase (Fig. 4*B*) and ACOX1 (Fig. 4*C*). Consistently, the formation of 4-HNE was enhanced in proximal tubules in WT mice after cisplatin treatment (Fig. 4*D*). These changes were attenuated in TG mice with cisplatin insults. These staining patterns were compatible with the results of pathological findings and TUNEL assay (Fig. 3, *C* and *D*, respectively).

Effects of Sirt1 Overexpression on Mitochondrial Number and Function in Cisplatin-induced AKI—As shown in Fig. 5*A*, cisplatin caused only a modest, albeit significant, decrease in mtDNA amounts (*i.e.* 13% reduction). Furthermore, the reduced mtDNA number was not restored in TG mice. The expression levels of PGC-1α, a key molecule for mitochondria proliferation, were markedly decreased in cisplatin-treated mice and were not ameliorated in TG mice (Fig. 5*B*). Cisplatin has also been reported to reduce the pro-

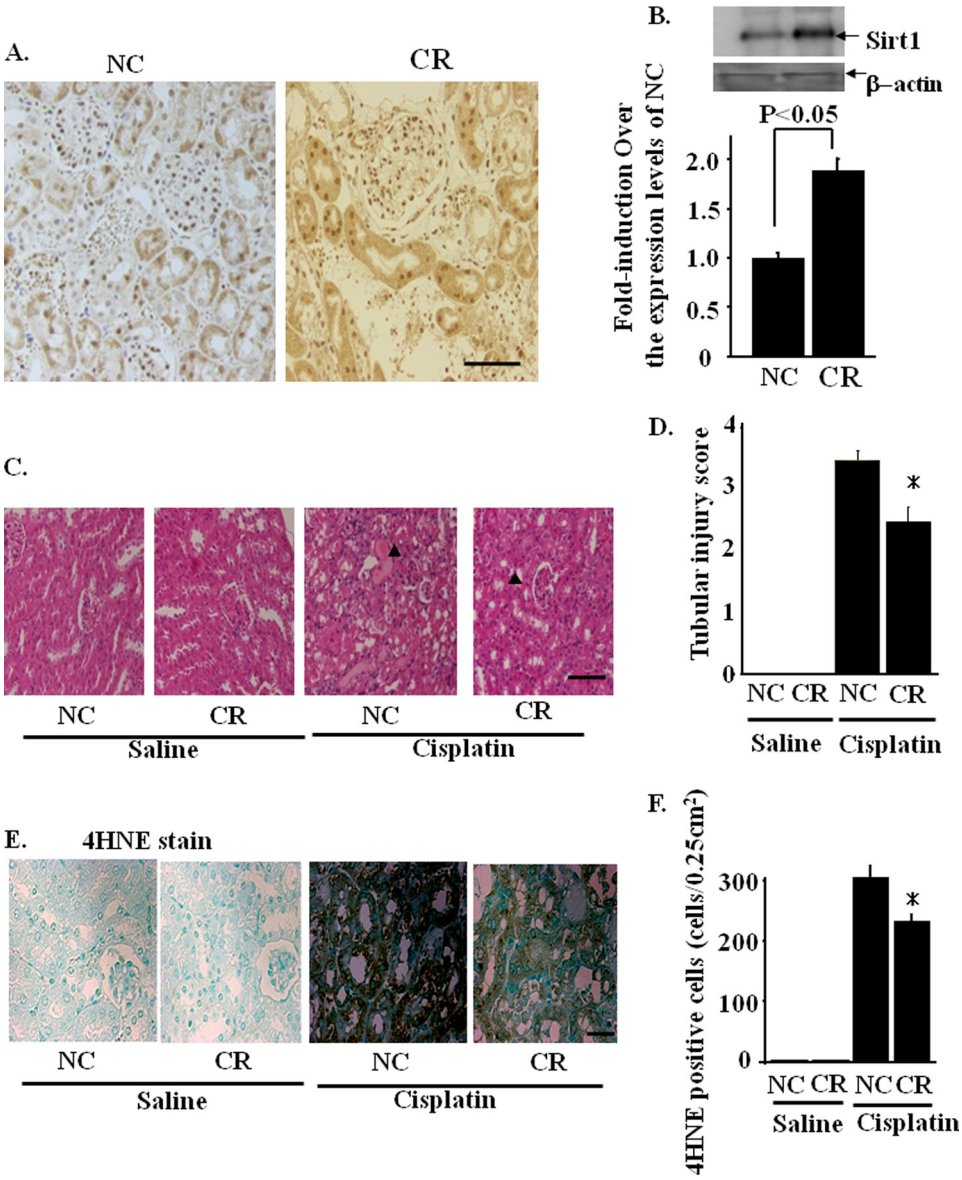

FIGURE 7. **Calorie restriction induced Sirt1 in the renal proximal tubules.** *A*, immunostaining with an anti-Sirt1 antibody shows increased Sirt1 staining in proximal tubules in mice on CR as compared with those in mice on NC. *Scale bar*, 50 μm. *B*, immunoblotting showed that Sirt1 protein expression was increased in kidneys of mice under CR for three months. *, $p < 0.05$ *versus* mice with NC ($n = 4$). *C* and *D*, effects of calorie restriction on cisplatin-induced acute kidney injury were examined as described under "Experimental Procedures." In mice on CR diet, the cisplatin-induced acute kidney injury was partially prevented, compared with that in mice on NC. *Scale bar*, 100 μm. The *arrowheads* indicate the areas of cisplatin-induced tissue damages. *E* and *F*, immunostaining against 4-HNE, a toxic lipid peroxidation product generated by the local H_2O_2, was prominent in mice on NC, but was diminished in mice on CR. *Scale bar*, 50 μm.

tein expression of MCAD, a rate-limiting enzyme in FAO in mitochondria. Similarly, a 52% decrease in MCAD expression was observed in WT mice compared with that in saline-injected mice (Fig. 5*C*). However, this alteration was partially reversed in TG mice.

Effects of Sirt1 Overexpression on the Activation of Downstream Transcription Factors—Sirt1 regulates the activities of various transcription factors involved in mitochondrial and peroxisomal function, including PPARα, PPARγ, and PGC-1α. The mRNA expressions of target genes of these molecules were examined by quantitative reverse transcription-PCR (supplemental Fig. SII). The mRNA levels of PPARα target genes, fatty acid transport proteins, and CYP4a10 were not affected by cisplatin treatment, which were not altered in TG mice, either. However, the mRNA levels of other PPARα target molecules, such as CPT1α, CPT1β, and (supplemental Fig. VA) were down-regulated by cisplatin, which were partially rescued in TG mice similarly with MCAD. The mRNA levels of PPARγ target genes, glycerol kinase, and glycerol-3-phosphate acetyltransferase were not altered by cisplatin treatment or by overexpression of Sirt1, which indicated that cisplatin-induced renal damages had no effect on PPARγ activity (supplemental Fig. SII). Consistent with the results of protein expression of PGC-1α (Fig. 5*B*), the mRNA levels of PGC-1α target genes (Atp5g1 and Cox5a) were decreased in WT mice treated with cisplatin and were not rescued in TG mice (supplemental Fig. SII).

Quantification of Peroxisome and Mitochondria on Immuno-EM in Cisplatin-induced AKI—To identify the peroxisomal or mitochondrial number in proximal tubular cells, immuno-EM was performed in the kidneys of WT and TG mice. The peroxisome membranes were positively stained with anti-PMP70 antibody, which allowed us to distinguish them from mitochondria. As shown in Fig. 6, both the number and the morphology of peroxisomes were not different between WT mice and TG mice with saline infusion. The insults with cisplatin reduced the number of peroxisomes in the kidney of WT mice and were restored in TG mice (WT *versus* TG; 9 ± 3 *versus* 22 ± 2 counts/micrograph; Fig. 6*B*). These results were comparable with the results of the expression levels of PMP70. The size and shape of peroxisomes in WT mice treated with cisplatin also changed; they were small with a serrated or indented contour. These morphological deformities were not observed in TG mice (Fig. 6*A*). Both the number and the morphology of mitochondria were not different between WT mice and TG mice with saline infusion. The insults with cisplatin slightly decreased the number of mitochondria in WT mice and were not reversed in TG mice (WT *versus* TG; 26 ± 3 *versus* 27 ± 2 counts/micrograph; Fig. 6*B*).

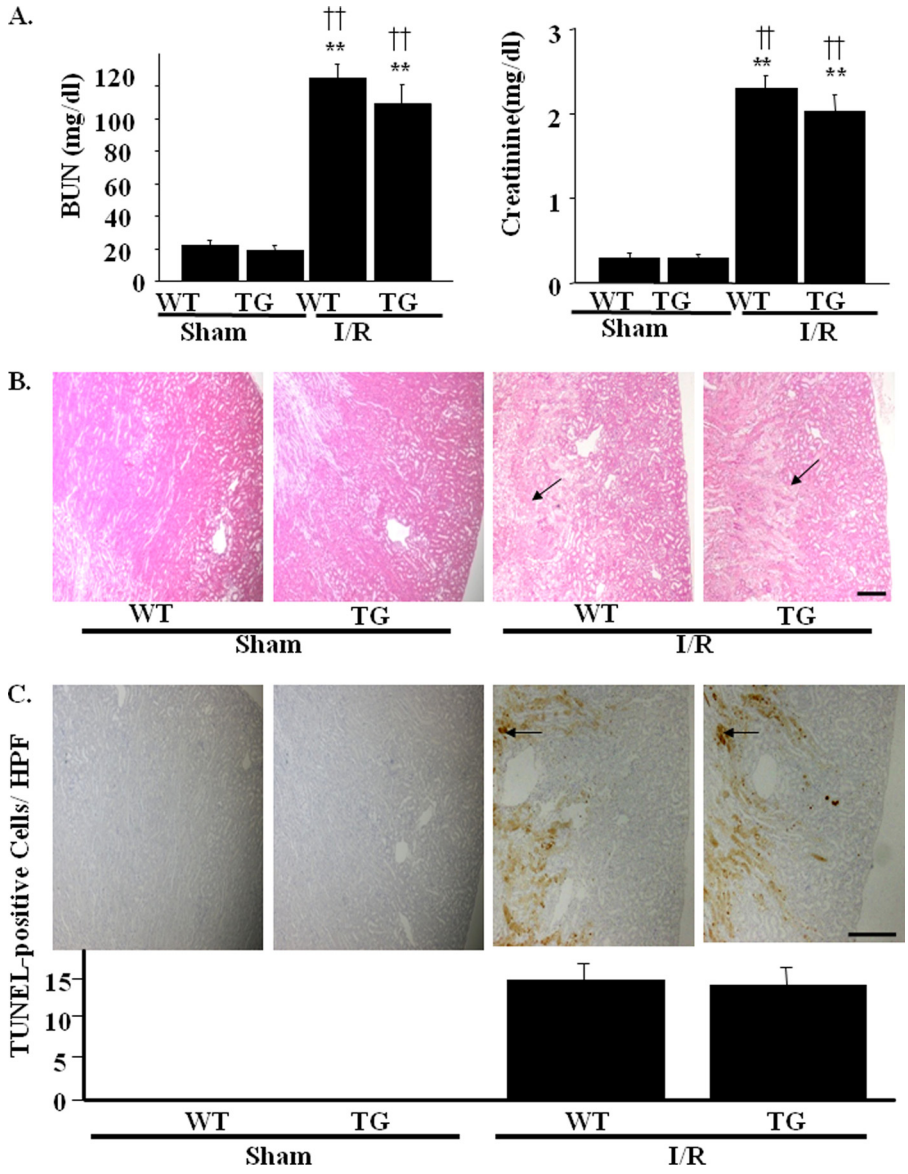

FIGURE 8. **Effects of kidney-specific Sirt1 overexpression on I/R-induced acute kidney injury.** WT or TG mice was assaulted by renal I/R as described under "Experimental Procedures." *A*, serum levels of BUN and creatinine were measured 24 h after I/R. *B*, pathological findings reveal extensive tubular damage with cast formation and many apoptotic bodies both in TG and WT mice. The *arrows* indicate the site of apoptotic bodies. *Scale bar*, 500 μm. *C*, representative images of TUNEL assay show I/R-induced renal tubular cell apoptosis in WT mice. The *arrows* indicate TUNEL-positive cells in high power field (×400, HPF) with condensed or fragmented nuclei. Similar levels of apoptotic cells are observed in kidneys from TG mice after I/R. *Scale bar*, 500 μm. **, $p < 0.01$ *versus* sham-operated WT mice; ††, $p < 0.01$ *versus* sham-operated TG mice ($n = 4$).

Effects of Calorie Restriction on Sirt1 Expression and Cisplatin-induced AKI—Because Sirt1 is an important factor that mediates the beneficial effects of calorie restriction (CR), we examined Sirt1 expression in the kidneys of mice on a 3-month CR diet. Immunohistochemistry in the kidneys in WT mice showed that there is clear nuclear staining in glomeruli and both nuclear and cytoplasmic staining in proximal tubules in WT mice. On the other hand, only faint expression of Sirt1 was detected in the distal tubules. As shown in the immunohistochemistry of the kidneys after CR (Fig. 7*A*), CR increases the Sirt1 expression in proximal tubules, whereas the Sirt1 expressions in glomeruli were not altered. Immunoblotting showed that renal Sirt1 expression was doubled in mice on CR as compared with that in mice fed normal chow (NC) (Fig. 7*B*). The renal protective role of CR in cisplatin-induced AKI was examined. In mice on NC, cisplatin aggravated renal function (BUN; 168 ± 21 *versus* 22 ± 4 mg/dl, $p < 0.01$, creatinine; 2.8 ± 0.3 *versus* 0.3 ± 0.1 mg/dl, $p < 0.01$) and produced marked renal histological changes. In contrast, in mice fed a CR diet, the changes in renal function were partially ameliorated (BUN, 115 ± 24 *versus* 19 ± 4 mg/dl, $p < 0.01$; creatinine, 2.1 ± 0.3 *versus* 0.3 ± 0.1 mg/dl, $p < 0.01$). Consistently, the renal histological changes induced by cisplatin were rescued significantly as compared with those in mice on NC (Fig. 7, *C* and *D*). Fig. 7*E* illustrates the effects of cisplatin on the production of 4-HNE in mice on NC and CR diets. Cisplatin markedly increased renal 4-HNE production in mice fed NC, which was partially restored in mice on a CR diet (Fig. 7, *E* and *F*). We further examined the effects of CR on the activation of downstream transcription factors of Sirt1 by quantitative reverse transcription-PCR. The mRNA expression of PPARα, PPARγ, and PGC-1α target genes, including MCAD and ACOX-1 was analyzed. These results were similar to those obtained in cisplatin-induced renal damages in TG mice (supplemental Figs. SIII and SIV).

Effects of Renal I/R Injury in Sirt1-TG Mice—We next examined the role of Sirt1 in renal I/R injury. Extensive tubular injuries were observed in WT kidneys 24 h after I/R. Overexpression of Sirt1, however, failed to protect against I/R injury. Neither renal function, as assessed by BUN and serum creatinine (Fig. 8*A*), nor renal histological findings were alleviated in Sirt1-TG mice, as compared with WT mice (Fig. 8*B*). Fig. 8*C* shows the effects of Sirt1 on the apoptotic process induced by I/R-induced AKI. Thus, I/R-induced TUNEL-positive cells were observed predominantly in the medulla rather than in the renal cortex, *i.e.* pereferentially in S3 segmental proximal tubules rather than in cortical proximal S1 or S2 segments. Kidneys in TG mice after I/R had nearly the same amount of TUNEL-positive cells as in WT mice (14.3 ± 3.2 *versus*13.7 ± 3.8 nuclei/high power field). In the immuno-EM, the number of peroxisomes was not affected by I/R, which were also unaltered in TG mice. On the other hand, the number of mitochondria was reduced by I/R, which was not ameliorated in TG

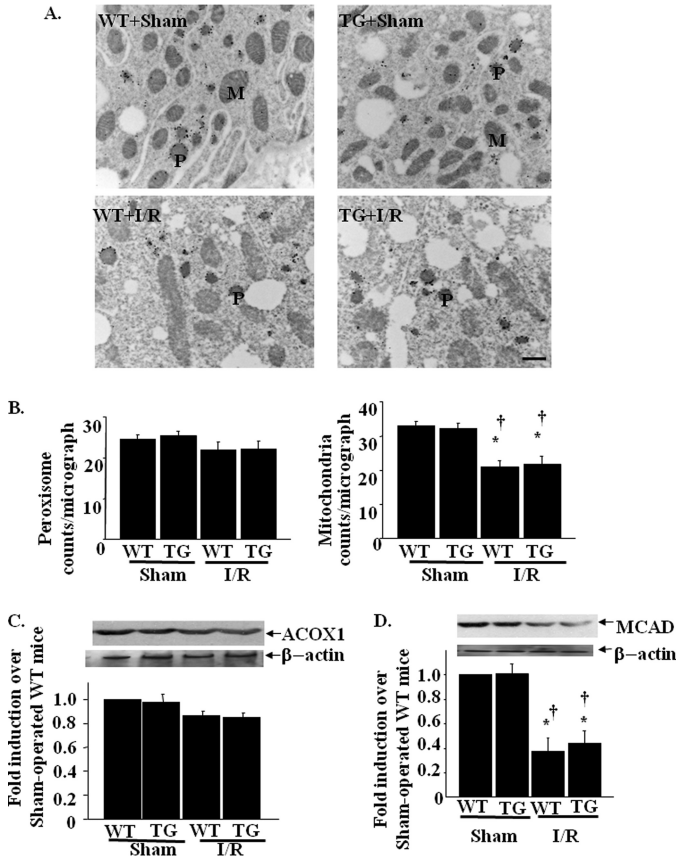

FIGURE 9. **Effects of kidney-specific Sirt1 overexpression on peroxisomal and mitochondrial in I/R-induced acute kidney injury.** *A*, kidney tissue sections were prepared for ultrastructural analysis by immuno-EM using anti-PMP70 antibody. Representative kidney histopathology from WT and TG mice with saline or cisplatin are shown. WT and TG mice with saline showed similar numbers of peroxisomes (*P*) and mitochondria (*M*). WT mice with cisplatin showed decreased numbers of peroxisome, which were alleviated in TG mice with cisplatin. *Scale bar*, 1 μm. *B*, peroxisomal and mitochondrial number in the micrograph at the magnification of $\times$ 12,800 were calculated as described under "Experimental Procedures." *, $p < 0.05$ *versus* saline-infused WT mice; ††, $p < 0.01$ *versus* saline-infused TG mice; §, $p < 0.05$ *versus* cisplatin-infused WT mice ($n = 8$). *C* and *D*, the expression levels of peroxisome protein, ACOX1 (*C*), and mitochondria protein MCAD (*D*) were analyzed by immunoblotting using kidney lysates from WT and TG mice after I/R-induced acute kidney injury. *, $p < 0.05$ *versus* sham-operated WT mice; †, $p < 0.05$ *versus* sham-operated TG mice ($n = 4$).

mice (Fig. 9, *A* and *B*). Western blotting using an anti-ACOX-1 antibody and an anti-MCAD antibody in I/R-induced AKI models showed that the protein levels of ACOX-1 were not affected by I/R, which were also unaltered by TG mice (Fig. 9*C*). The protein levels of MCAD were decreased by I/R and were not ameliorated by TG mice (Fig. 9*D*). These data indicated that I/R mainly damaged mitochondria, which was resistant to the effects by Sirt1 overexpression.

The Effects of Sirt1 Overexpression on Cisplatin or I/R-induced Cellular Damages in HK-2 Cells—We examined the direct effects of cisplatin or I/R on peroxisomal or mitochondrial number in proximal tubular cells. We first confirmed that both 50 μM cisplatin treatment for 24 and 12 h after I/R models caused cellular apoptosis to a similar extent, showing a similar percentage of the population of cells stained with annexin V, a marker of apoptotic changes (Fig. 10*A*). In the assay for peroxisomal number by Peroxi-GFP fluorescence, the expression of Sirt1 prevented the decrease in peroxisome number induced by cisplatin treatment (Fig. 10*B*). However, in the assay for mitochondria number by Mito-OFP fluorescence, Sirt1 did not alter the reduction in mitochodria number induced by I/R (Fig. 10*C*). These results are consistent with the results in cisplatin-induced AKI as well as in I/R-induced AKI. The present results also suggest that Sirt1 overexpression results in cisplatin-induced peroxisomal number reduction directly.

DISCUSSION

Although cisplatin is clinically used as an anti-cancer therapy, nephrotoxicity remains a critical problem. Pathologically, cisplatin is demonstrated to elicit predominantly proximal tubular injury. Previous investigations demonstrated that resveratrol up-regulated Sirt1 expression (23) and attenuated the cisplatin-induced AKI (24). In concert, these observations lend support to the hypothesis that the modulation of Sirt1 expression constitutes a molecular tool for the prevention of cisplatin-induced AKI.

The mechanism for the protective action of Sirt1 on cisplatin-induced AKI has not been assessed hitherto. It has been reported that cisplatin affects the peroxisome system, including the suppression of peroxisome number and function in kidney tissues of mice (11). The peroxisome is an organelle bound by a single membrane and is involved in metabolic processes, including peroxide-based respiration and oxidative degradation of fatty acids and purines (25). Furthermore, peroxisome eliminates excessive ROS and promotes FAO that is closely linked to the key system for ATP generation. The present study demonstrates that cisplatin causes a decrease in peroxisome number (*i.e.* PMP70; Fig. 4*A*) whose function as evaluated by a reduction in catalase expression (Fig. 4*B*) as well as the expression of ACOX1, a member of FAO systems (Fig. 4*C*) and the subsequent accumulation of 4-HNE (Fig. 4*D*). All of these parameters are well preserved in kidneys from TG mice. Indeed, we have recently demonstrated that Sirt1 prevents apoptosis through the induction of catalase in HK-2 cells (7). Catalase is located in peroxisome fraction, which has been shown to promote peroxisome proliferation (26); the supplementation of peroxisome activator nafenopin results in a sustained increase in the number of peroxisomes with concomitant increases in catalase activity (27). Increased catalase therefore may eliminate H_2O_2 within peroxisome, which possibly leads to the mitigation of the damages to peroxisome. Therefore, it appears that the protective effects of Sirt1 on the peroxisome enzyme are partially secondary to the induction of catalase and/or its resultant peroxisome proliferation. In concert, our study reveals that peroxisome is an important intracellular target organelle for Sirt1.

Mitochondria are important organelles for the maintenance of vital function. It has been reported that mitochondria are altered in both number and function in cisplatin-induced AKI (12). In AKI, the elevated ROS level within mitochondria is deleterious to the cell because of their ability to induce lipid peroxidation, protein oxidation, and DNA damage. The increased ROS also damages mitochondria, which subsequently produces excessive ROS (28). In the present study, cisplatin injection reduces both mitochondrial DNA copy number

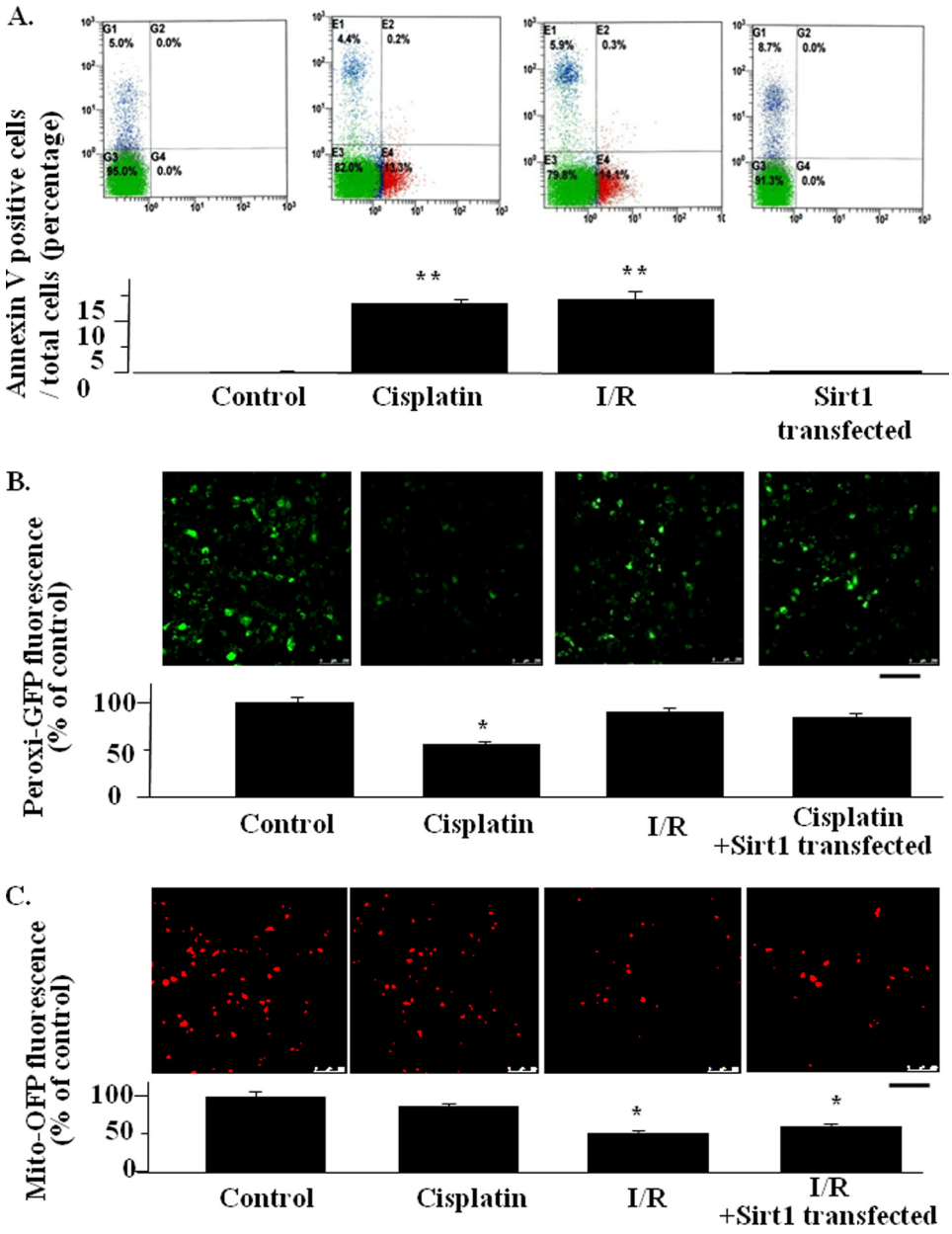

FIGURE 10. **Effects of Sirt1 overexpression on peroxisome and mitochondria mass in HK-2 cells.** *A*, apoptosis was determined by FACS. Each graph for FACS represents the population of the cells stained with annexin V (*x axis*) and propiumiodine (*y axis*) (*upper panel*). A *bar graph* summarizing the FACS results are shown in the *lower panel*. The data are the means ± S.E. *, $p < 0.05$ *versus* control. All of experiments were conducted three times using different cultures. *B* and *C*, representative confocal laser scanning microscopic images of Peroxi-GFP, for the assessment of peroxisome number (*B*) and Mito-OFP, for the assessment of mitochondrial number (*C*), in HK2 cells with or without cisplatin treatment or I/R model. The bar graph under each microscopic image represents the quantification of the average pixel intensity of Peroxi-GFP (*B*) or Mito-OFP (*C*). *, $p < 0.05$ *versus* untreated control cells ($n = 4$). *Scale bars*, 50 μm.

and PGC-1α, a principle regulator for mitochondria biogenesis (Fig. 5, *A* and *B*). Nevertheless, TG mice did not exhibit the reversal of mitochondrial DNA copy number or PGC-1α expression. Alternatively, whereas cisplatin down-regulated the expression of mitochondria enzyme, MCAD, Sirt1 overexpression restored the MCAD expression, thus suggesting that mitochondria function was partially recovered by Sirt1 overexpression (Fig. 5*C*). Furthermore, as shown in 4-HNE staining (Fig. 4*D*), overexpression of catalase is capable of reducing H_2O_2 in peroxisome, which would diminish the cellular ROS and subsequently restore the mitochondrial β-oxidation enzyme system (Fig. 5*C*), with resultant ATP generation (Fig. 10). Because our cell culture study revealed that Sirt1 did not modify the mitochondrial number directly, the reversal of mitochondrial enzyme in TG mice was a secondary effect of the reduction in cellular ROS through the activation of the Sirt1-catalase system (Fig. 11).

The results of immuno-EM supported these results. Cisplatin induced the reduction in the number and morphological deformities of peroxisomes, which were reversed by Sirt1 overexpression. These changes *in vivo* are due to the direct effect of cisplatin and Sirt1 overexpression because these data are also consistent with the result of the *in vitro* study using HK-2 cells. However, the precise mechanism for the protective effect of Sirt1 on the morphological changes of peroxisomes needs to be examined. In contrast, mitochondrial number on immuno-EM was not altered with cisplatin, whereas mtDNA copy number was slightly changed, and PCG1α was remarkably reduced with cisplatin. This may suggest that the early biochemical changes such as PGC-1α, which preceded the morphological alterations (*i.e.* mtDNA copy number and mitochondria number observed on EM) were detected earlier in this model. Moreover, neither mtDNA copy number nor PCG1α were affected by Sirt1 overexpression.

Renal I/R injury is also a serious problem among AKI. Previous studies documented that peroxisome number and/or function were damaged in the kidneys of mice undergoing I/R injury (13). In the present study, however, we failed to demonstrate a beneficial effect of Sirt1 on the development of AKI when induced by I/R injury (Fig. 8, *A* and *B*). The reason for this observation is most likely explained by the difference in the affected cellular organellae between by the cisplatin insults and by I/R injury. Cisplatin mainly damaged peroxisomes as evident in immuno-EM (Fig. 6), whereas I/R did not affect peroxisomes much but damaged mitochondria predominantly (Fig. 9). Because Sirt1 rescues renal tubular damages mainly through the restoration of peroxisome number and function, Sirt1 may not be able to rescue

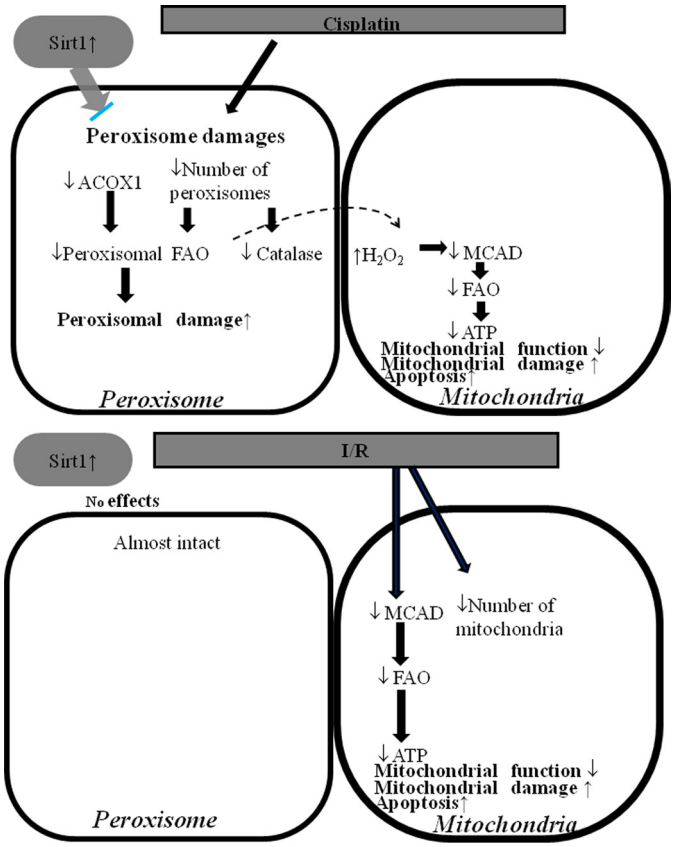

FIGURE 11. **Schematic diagram illustrating the effects of cisplatin on peroxisome and mitochondria function and the protective role of Sirt1.** Cisplatin decreased the number of peroxisomes resulting in a decrease in FAO activity and catalase expression. Sirt1 overexpression maintained peroxisome and alleviates the cisplatin-induced acute kidney injury. I/R caused mitochondrial insult, which lead to decreasing the number of mitochondria and a concomitant decrease in the expression levels of mitochondrial enzymes. Sirt1 overexpression could not rescue I/R-induced damages because Sirt1 had no effects on mitochondria number and function.

the damage caused by I/R because I/R may not affect peroxisomes much. These selective effects by Sirt1 were also confirmed by our *in vitro* experiments (Fig. 10). We next examined the molecular mechanisms for the preservation of the number and function of peroxisome. We previously demonstrated that, in HK-2 cells, overexpression of Sirt1 protects against oxidative stress-induced cellular apoptosis by FoxO3a-mediated up-regulation of catalase (7). This was effective in cisplatin-induced renal ROS increase but might not be efficient in the renal survival in I/R-induced ROS production. In I/R-induced AKI, the expressions of catalase were not altered, nor were they altered in TG mice (data not shown). These data implied that other ROS scavengers such as glutathione peroxidase and superoxide dismutase, but not catalase, might play an important role in eliminating excessive ROS produced by I/R-induced AKI. In fact, the renal protective effects of these two ROS scavengers against I/R-induced renal damages have already been reported in the previous paper (29, 30). To explore the molecular mechanism for the renal protective effects by Sirt1, we next investigated the effects on PPARα and PPARγ activity. Although several target genes of PPARγ, including glycerol kinase and glycerol-3-phosphate acetyltransferase, were not altered (supplemental Fig. SII), several PPARα target genes, including ACOX1, MCAD (both Figs. 4 and 5), CPT1α, and CPT1β (supplemental Fig. SV*A*), were restored by Sirt1 overexpression. However, these changes were not observed in I/R-induced renal damages (supplemental Fig. SV*B*). These results implied that the renal protective effects by Sirt1 might not conferred mainly by the activation of PPARα.

Although the current study shows the role of Sirt1 in AKI induced by cisplatin and/or I/R injury in Sirt1-TG mice, the ability to manipulate this factor and modify the course of AKI is undetermined. CR is applied as a widespread useful tool for Sirt1 up-regulation (31). In the present study, we have demonstrated that CR elevates Sirt1 protein expression in proximal tubules, particularly in cortical segments (1.8-fold increase; Fig. 7*B*). In this setting, renal pathological changes as well as lipid peroxidation products were significantly suppressed, compared with those observed in mice on NC (Fig. 7, *D* and *F*). However, further investigations are required to establish the clinical relevance of CR in the prevention of AKI.

The whole body Sirt1 knock-out mice showed early postnatal lethality and exhibited heart and retinal developmental defects (32). TG mice overexpressing Sirt1 in the whole body exhibited similar phenotypes as calorie-restricted mice, including lower body weight, reduction of fat mass, lower level of total blood cholesterol, and improved glucose tolerance (33). As for conditional knock-out mice for Sirt1, liver-specific knock-out mice showed improved glucose tolerance (34). As for conditional TG mice, the results of pancreatic-specific (34), endothelial cell-specific (35), and cardiac muscle-specific (6) mice have shown that Sirt1 overexpression in each tissue exerted organ-protective effects. Despite these studies, the phenotypes of knock-out or TG mice specifically targeted in the kidney have not been reported thus far. The present study is the first investigation that elucidated the function of Sirt1 in kidney *in vivo*.

In conclusion, we have demonstrated that renal Sirt1 exerts protective action on AKI, possibly because of the preservation of peroxisome functions. These effects contributed substantially to the elimination of excessive ROS and to the recovery from mitochondria dysfunction. Our results provide firm evidence that the modalities modulating Sirt1 activity constitute attractive candidates for the treatment of peroxisome dysfunction-related AKI.

REFERENCES

1. Guarente, L. (2000) *Genes Dev.* **14,** 1021–1026
2. Luo, J., Nikolaev, A. Y., Imai, S., Chen, D., Su, F., Shiloh, A., Guarente, L., and Gu, W. (2001) *Cell* **107,** 137–148
3. Nemoto, S., Fergusson, M. M., and Finkel, T. (2004) *Science* **306,** 2105–2108
4. Wiggins, J. E., Goyal, M., Sanden, S. K., Wharram, B. L., Shedden, K. A., Misek, D. E., Kuick, R. D., and Wiggins, R. C. (2005) *J. Am. Soc. Nephrol.* **16,** 2953–2966
5. Giovannini, L., Migliori, M., Longoni, B. M., Das, D. K., Bertelli, A. A., Panichi, V., Filippi, C., and Bertelli, A. (2001) *J. Cardiovasc. Pharmacol.* **37,** 262–270
6. Alcendor, R. R., Gao, S., Zhai, P., Zablocki, D., Holle, E., Yu, X., Tian, B., Wagner, T., Vatner, S. F., and Sadoshima, J. (2007) *Circ. Res.* **100,** 1512–1521
7. Hasegawa, K., Wakino, S., Yoshioka, K., Tatematsu, S., Hara, Y., Minakuchi, H., Washida, N., Tokuyama, H., Hayashi, K., and Itoh, H. (2008) *Biochem. Biophys. Res. Commun.* **372,** 51–56
8. Brezniceanu, M. L., Liu, F., Wei, C. C., Chénier, I., Godin, N., Zhang, S. L.,

Filep, J. G., Ingelfinger, J. R., and Chan, J. S. (2008) *Diabetes* **57,** 451–459
9. Purushotham, A., Schug, T. T., Xu, Q., Surapureddi, S., Guo, X., and Li, X. (2009) *Cell Metab.* **9,** 327–338
10. Elliott, P. J., and Jirousek, M. (2008) *Curr. Opin. Investig. Drugs* **9,** 371–378
11. Negishi, K., Noiri, E., Sugaya, T., Li, S., Megyesi, J., Nagothu, K., and Portilla, D. (2007) *Kidney Int.* **72,** 348–358
12. Santos, N. A., Catão, C. S., Martins, N. M., Curti, C., Bianchi, M. L., and Santos, A. C. (2007) *Arch. Toxicol.* **81,** 495–504
13. Gulati, S., Singh, A. K., Irazu, C., Orak, J., Rajagopalan, P. R., Fitts, C. T., and Singh, I. (1992) (1992) *Arch. Biochem. Biophys.* **295,** 90–100
14. Plotnikov, E. Y., Kazachenko, A. V., Vyssokikh, M. Y., Vasileva, A. K., Tcvirkun, D. V., Isaev, N. K., Kirpatovsky, V. I., and Zorov, D. B. (2007) *Kidney Int.* **72,** 1493–1502
15. Nisoli, E., Tonello, C., Cardile, A., Cozzi, V., Bracale, R., Tedesco, L., Falcone, S., Valerio, A., Cantoni, O., Clementi, E., Moncada, S., and Carruba, M. O. (2005) *Science* **310,** 314–317
16. Brunet, A., Sweeney, L. B., Sturgill, J. F., Chua, K. F., Greer, P. L., Lin, Y., Tran, H., Ross, S. E., Mostoslavsky, R., Cohen, H. Y., Hu, L. S., Cheng, H. L., Jedrychowski, M. P., Gygi, S. P., Sinclair, D. A., Alt, F. W., and Greenberg, M. E. (2004) *Science* **303,** 2011–2015
17. Rosenberg, T., Shachaf, C., Tzukerman, M., and Skorecki, K. (2007) *Am. J. Physiol. Renal Physiol.* **292,** F1617–F1625
18. Hasegawa, K., and Nakatsuji, N. (2002) *FEBS Lett.* **520,** 47–52
19. Wakino, S., Kintscher, U., Liu, Z., Kim, S., Yin, F., Ohba, M., Kuroki, T., Schönthal, A. H., Hsueh, W. A., and Law, R. E. (2001) *J. Biol. Chem.* **276,** 47650–47657
20. Vicari, A. P., Figueroa, D. J., Hedrick, J. A., Foster, J. S., Singh, K. P., Menon, S., Copeland, N. G., Gilbert, D. J., Jenkins, N. A., Bacon, K. B., and Zlotnik, A. (1997) *Immunity* **7,** 291–301
21. Hashiguchi, N., Kojidani, T., Imanaka, T., Haraguchi, T., Hiraoka, Y., Baumgart, E., Yokota, S., Tsukamoto, T., and Osumi, T. (2002) *Mol. Biol. Cell* ***13***, 711–722
22. van Hoek, A. N., Ma, T., Yang, B., Verkman, A. S., and Brown, D. (2000) *Am. J. Physiol. Renal Physiol.* **278,** F310–F316
23. Wood, J. G., Rogina, B., Lavu, S., Howitz, K., Helfand, S. L., Tatar, M., and Sinclair, D. (2004) *Nature* **430,** 686–689
24. Do Amaral, C., Francescato, H. D., Coimbra, T. M., Costa, R. S., Darin, J. D., Antunes, L. M., and Bianchi, M. L. (2008) *Arch. Toxicol.* **82,** 363–370
25. Schrader, M., and Fahimi, H. D. (2006) *Biochim. Biophys. Acta* **1763,** 1755–1766
26. Zhou, Z., and Kang, Y. J. (2000) *J. Histochem. Cytochem.* **48,** 585–594
27. Lawrence, J. W., Foxworthy, P. S., Perry, D. N., Jensen, C. B., Giera, D. D., Meador, V. P., and Eacho, P. I. (1995) *Biochem. Pharmacol.* **49,** 915–919
28. Rasbach, K. A., and Schnellmann, R. G. (2007) *J. Biol. Chem.* **282,** 2355–2362
29. Tenorio-Velázquez, V. M., Barrera, D., Franco, M., Tapia, E., Hernández-Pando, R., Medina-Campos, O. N., and Pedraza-Chaverri, J. (2005) *BMC Nephrol.* **6,** 12
30. Kim, J., Kil, I. S., Seok, Y. M., Yang, E. S., Kim, D. K., Lim, D. G., Park, J. W., Bonventre, J. V., and Park, K. M. (2006) *J. Biol. Chem.* **281,** 20349–20356
31. Chen, D., Steele, A. D., Lindquist, S., and Guarente, L. (2005) *Science* **9,** 1641
32. Cheng, H. L., Mostoslavsky, R., Saito, S., Manis, J. P., Gu, Y., Patel, P., Bronson, R., Appella, E., Alt, F. W., and Chua, K. F. (2003) *Proc. Natl. Acad. Sci. U.S.A.* **100,** 10794–10799
33. Bordone, L., Cohen, D., Robinson, A., Motta, M. C., van Veen, E., Czopik, A., Steele, A. D., Crowe, H., Marmor, S., Luo, J., Gu, W., and Guarente, L. (2007) *Aging Cell* **6,** 759–767
34. Moynihan, K. A., Grimm, A. A., Plueger, M. M., Bernal-Mizrachi, E., Ford, E., Cras-Méneur, C., Permutt, M. A., and Imai, S. (2005) *Cell Metab.* **2,** 105–117
35. Zhang, Q. J., Wang, Z., Chen, H. Z., Zhou, S., Zheng, W., Liu, G., Wei, Y. S., Cai, H., Liu, D. P., and Liang, C. C. (2008) *Cardiovasc Res.* **80,** 191–199